Engineering Structures 281 (2023) 115781

Contents lists available at ScienceDirect

Engineering Structures

journal homepage: www.elsevier.com/locate/engstruct

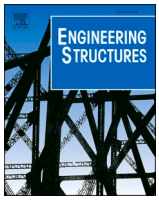

Seismic assessment and dissipative bracing retrofit-based protection of infills and partitions in RC structures

Stefano Sorace [a,*], Iacopo Costoli [a], Gloria Terenzi [b]

[a] Polytechnic Department of Engineering and Architecture, University of Udine, Via delle Scienze 206, 33100 Udine, Italy
[b] Department of Civil and Environmental Engineering, University of Florence, Via S. Marta 3, 50139 Florence, Italy

ARTICLE INFO

Keywords:
Infills
Partitions
Seismic damage
Seismic retrofit
Dissipative braces
Fluid viscous dampers

ABSTRACT

A balanced performance improvement of the constituting structural members, infills and partitions is a fundamental requirement in seismic retrofit design of frame buildings. In order to pursue this objective, the response of the non-structural elements must be accurately simulated, so as to evaluate their damage evolution and the correlation with the response of the structural skeleton. In the study presented in this article, diagonal no-tension struts with multilinear "pivot"-type hysteretic behaviour are adopted as substitute elements for masonry infill and partition panels. A trilinear axial force–displacement backbone curve is generated for the equivalent struts and transformed in the lateral force-drift curve of the panels. The latter is then scanned in terms of sequential performance limits and ranges. This model is demonstratively applied to a real case study, i.e. a reinforced concrete frame building damaged by the 2016 Central Italy earthquake, although a retrofit intervention had been carried out a few years before. Based on the results of the time-history assessment analyses in its original conditions, an alternative retrofit solution is proposed, consisting in the incorporation of dissipative braces equipped with pressurized fluid viscous dampers. This technology was selected for its high-damping capacity, as well as for the prompt activation of the constituting devices starting from the early stages of the building seismic response. The verification analyses developed in retrofitted configuration for the main shock records of the 2016 earthquake confirm this property, showing slight damage only in a small number of partitions—instead of the diffused moderate-to-irreparable damage actually surveyed in the building partitions and infills—and safe response of all structural members.

1. Introduction

The design of seismic retrofit interventions on frame buildings involves, like for new buildings, a comprehensive control of their response capacities for the four reference hazard levels established by most Technical Standards, i.e. Frequent Design Earthquake (FDE), Serviceability Design Earthquake (SDE), Basic Design Earthquake (BDE) and Maximum Considered Earthquake (MCE). Nonetheless, the earthquakes occurred in the last decade have sometimes highlighted unsatisfactory responses of non-structural components, and particularly of infills and partitions, in recently retrofitted buildings, although an adequate protection of the structure has been normally observed [1–2]. This urges to properly simulate the response of infills and partitions in retrofit design analyses, as well as to evaluate how these retrofitted buildings would have responded should a different rehabilitation strategy have been adopted for them.

This topic is developed in the study presented herein, where a representative building is examined, i.e. a school with reinforced concrete (RC) structure situated in the municipality of Norcia, Umbria, Italy. The building was seismically retrofitted in 2013 by adding buckling restrained braces in some perimeter alignments of the above-ground storeys. In spite of these rehabilitation measure, remarkable damage to a wide portion of its clay brick masonry partitions and infills was caused by the 2016 Central Italy earthquake. Indeed, the post-quake surveys and relevant assessment studies carried out on the building [3–5] have highlighted a delayed activation of the supplemental damping action of the buckling restrained braces, as a consequence of the high stiffness of the incorporated metallic yielding devices. In particular, it has been estimated that they responded like traditional non-dissipative braces up to an input acceleration value of about 0.2 g. In doing so, an about 15 % reduction of inter-storey drifts was reached in the upper storeys before exceeding this acceleration threshold, counterbalanced by a comparable increase in storey shears. In view of this, the system failed to protect

* Corresponding author.
E-mail addresses: stefano.sorace@uniud.it (S. Sorace), iacopo.costoli@uniud.it (I. Costoli), gloria.terenzi@unifi.it (G. Terenzi).

https://doi.org/10.1016/j.engstruct.2023.115781
Received 2 May 2022; Received in revised form 2 February 2023; Accepted 5 February 2023
Available online 15 February 2023

Nomenclature

List of symbols

$\|\cdot\|$	absolute value
b_s	width of equivalent strut element
c	damping coefficient of PFV damper
d_s	length of equivalent strut element
f	stiffness degradation parameter in hysteretic model of equivalent strut element
f_{js}	sliding resistance of mortar joints of infill or partition panel
f_{pd}	shear resistance of infill or partition panel under diagonal compression
f_{pv}	compressive strength of infill or partition panel
h_i	inter-storey frame height
h_{mp}	height of infill or partition panel
k_1, k_2	first and second branch stiffness of elastic response component of PFV damper
$sgn(\cdot)$	signum function
t	time variable
t_{mp}	thickness of infill or partition panel
$x(t)$	displacement of PFV damper
$\dot{x}(t)$	velocity of PFV damper
D_p	drift of infill or partition panel
D_{pr}	ratio of infill or partition panel drift to h_i
D_s	axial displacement of equivalent strut element
E_c	Young modulus of material constituting columns adjacent to infill or partition panel
$E_{d,sd}$	energy dissipated by PFV damper
$E_{d,t}$	total dissipated energy
$E_{i,t}$	total seismic input energy
E_{mh}, E_{mv}	Young moduli of masonry in horizontal and vertical direction
$E_{m\phi}$	Young modulus of masonry in direction parallel to equivalent strut element
E_n	nominal energy dissipation capacity of PFV damper
F_d, F_e	damping and elastic reaction force components of PFV damper
F_0	static pre-load of PFV damper
G	shear modulus of masonry
H_p	lateral force of infill or partition panel
$H_{p,cr}$	cracking H_p value
$H_{p,\max}$	maximum H_p value
$H_{p,c}$	residual H_p value
H_s	axial force of equivalent strut element
$H_{s,\max}$	maximum H_s value
I_c	moment of inertia of columns adjacent to infill or partition panel calculated about normal axis to panel
K_1, K_2	empirical coefficients
l_i	centerline length of frame span where infill or partition panel is included
t_s	thickness of equivalent strut element
ε_s	axial strain of equivalent strut element
$\varepsilon_{s,abl}$	axial strain of equivalent strut element corresponding to $\sigma_{s,\max}$
γ	fractional exponent of velocity of PFV damper
λ	multiplying factor of h_i for the evaluation of b_s
λh_i	non-dimensional parameter, function of geometrical and mechanical characteristics of frame-panel system
ν	Poisson ratio of masonry
$\sigma_{p,\min}$	minimum stress value among σ_{p1}, σ_{p2}, σ_{p3} and σ_{p4}
σ_{p1}, σ_{p2}, σ_{p3}, σ_{p4}	stress values associated with the achievement of compression in the middle (σ_{p1}), compression at the corners (σ_{p2}), shear-sliding (σ_{p3}) and shear-diagonal crack (σ_{p4}) infill or partition panel collapse mechanisms
σ_s	axial stress in equivalent strut element
$\sigma_{s,\max}$	maximum σ_s value
σ_v	vertical compression stress in infill or partition panel
ϕ	inclination angle of equivalent strut with respect to the horizontal axis

partitions and infills, which started to be damaged below this acceleration level due to their typical interaction with the structural skeleton [6]. At the same time, the activation of the steel dissipators occurred for the subsequent highest acceleration peaks helped substantially protect the RC structure, with light-to-moderate plasticizations of the most stressed beams and columns [3–5], consistently with typical performance capacities of several types of metallic dampers [7–10].

Based on these observations, an alternative retrofit strategy is proposed for the building, which consists in the incorporation of a dissipative bracing system equipped with pressurized fluid viscous (PFV) dampers. This system was devised and applied in previous studies by the authors to several different types of buildings, including schools [11–16]. In order to carefully evaluate the response of infills and partitions in the assessment and design analyses, these elements are modelled by means of diagonal no-tension struts with multilinear pivot-type hysteretic behaviour. A trilinear axial force–displacement backbone curve is defined for the equivalent struts, which is subsequently transformed in the lateral force-drift curve of the panels. The latter is divided into nine sub-branches by identifying a set of sequential performance ranges and relevant limits, extracted and elaborated from experimental and numerical literature studies.

The time-history assessment analysis developed on the structure in the conditions preceding the installation of the buckling restrained braces, the construction of the backbone curve of infill and partition panels, the design of the PFV-dissipative bracing system, and the verification analyses in the presence of the latter are presented in the next Sections.

2. Case study building

The case study school was built in Norcia, Umbria, Italy in the early 1960s, with a (59.6 × 12.9) m^2 sized rectangular plan (Fig. 1), and is composed of a basement, three above-ground storeys and a gable roof. As shown in the longitudinal cross section of Fig. 1, the inter-storey heights are equal to 3.5 m (basement) and 3.3 m (above-ground). Fig. 2 shows the structural plans of the above-ground storeys with the alphanumerical identification of the fixed alignments. The floors and roof are made of 160 mm-thick RC joists parallel to the X axis of the reference coordinate system, shown in Fig. 1, with interposed clay lug bricks and a 40 mm-thick upper RC slab. The latter guarantees a sufficient diaphragm-like in-plane stiffness of floors in the transmission of story shears. The frame structure is a RC skeleton, with primary beams situated in the alignments parallel to Y (numbered 1–18 in Fig. 2). A set of eight steel braces made of HEA 200 profiles was introduced in 2005 in the C longitudinal alignment of the basement, as highlighted by red segments in the plan and section of Fig. 1 too. The HEA 200 trusses were connected to the beam-to-column joints by means of bolted L-shaped steel plates. This local intervention was conceived as a first-level retrofit solution after the 2003 reclassification of the municipality of Norcia as a higher seismicity zone, as compared to the previous categorization dating back to 1996. The design objective was to compensate for the elimination of some thick partitions on the basement caused by an architectural reorganization of relevant spaces, which emphasized the greater lateral deformability of this storey in X direction.

The cross sections of beams and columns are detailed in Figs. 3 and 4,

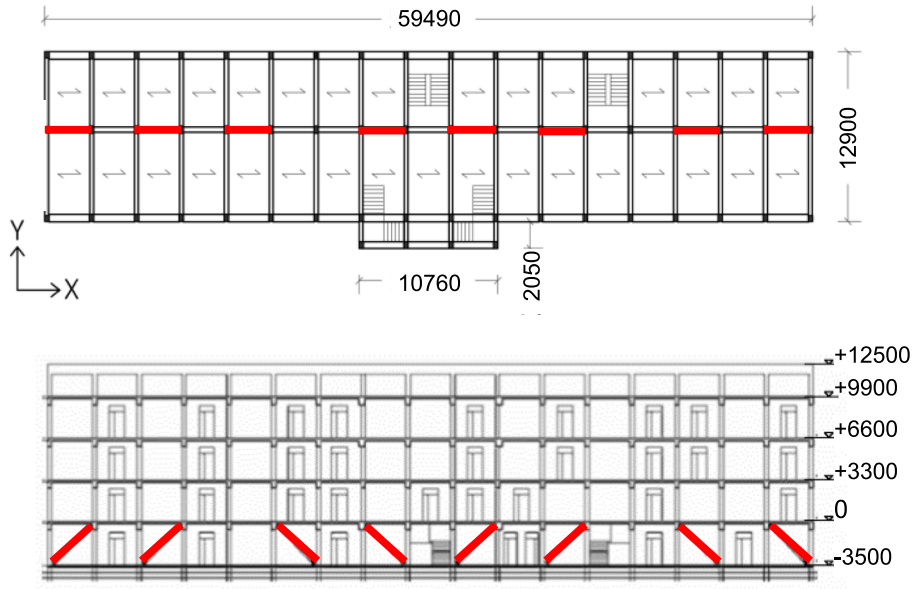

Fig. 1. Structural plan of the above-ground storeys and longitudinal section of the building (dimensions in mm), with highlighted in red the conventional steel braces installed in 2005. (For interpretation of the references to colour in this figure legend, the reader is referred to the web version of this article.)

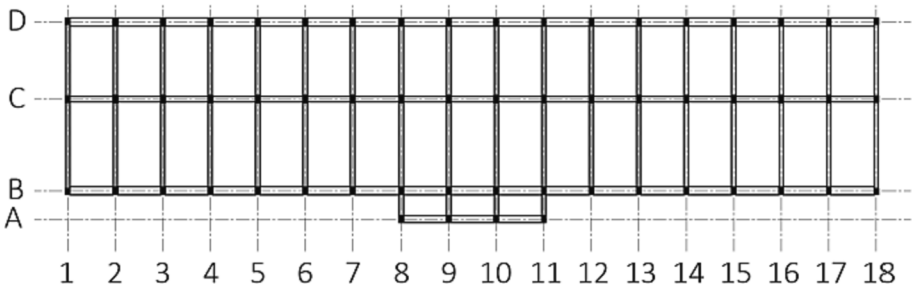

Fig. 2. Fixed alignments of the structural plan of the above-ground storeys.

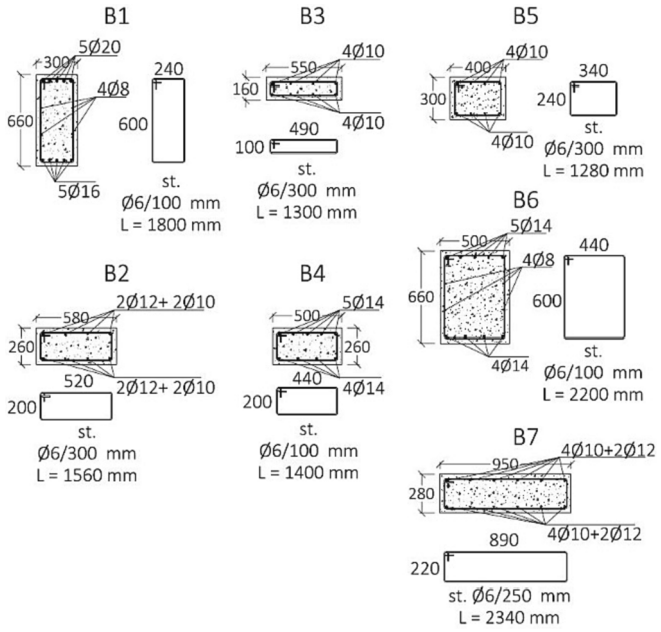

Fig. 3. Beam sections (dimensions in mm).

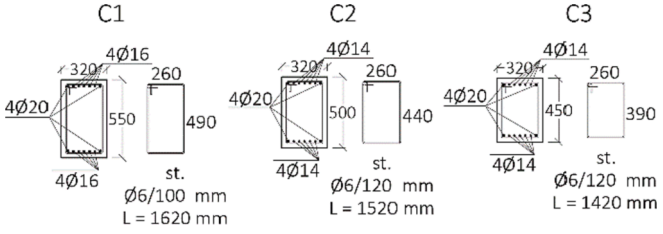

Fig. 4. Column sections (dimensions in mm).

respectively. The storey and alignment locations of all members are recapitulated in Tables 1 and 2. As highlighted by the structural plan in Fig. 1, as well as by the drawings in Fig. 3 and the data in Table 1, all primary beams (B1 type) have an identical massive out-of-depth section, sized (300 × 660) mm^2. This is a consequence of the fact that, although not a mandatory requirement in the Technical Standards of the time, the structural design was carried out by considering an equivalent static distribution of lateral seismic forces parallel to Y, scaled by a seismic coefficient (given by the ratio of the sum of the seismic forces to the building weight) equal to 0.07. In spite of the relatively low value assumed for this coefficient, the simplified seismic design provided a rather high translational stiffness and a moderate seismic resistance to the frame structure in transversal direction. On the other hand, no lateral seismic force distribution was considered in X, which caused to obtain all in-depth beam sections in the longitudinal direction (B2, B3,

Table 1
Beam locations in plan and elevation.

Storey	Alignments	Beam section types
Basement	A	B4
	B, D	B2
	C	B3
	1 – 18	B1
Ground	A	B6
	B, D	B2
	C	B5
	1–18	B1
First	A	B6
	B, D	B2
	C	B5
	1–18	B1
Second	A	B7
	B, D	B7
	C	B5
	1–18	B1

Table 2
Column locations in plan.

Storey	Alignments	Column section types
Basement	A, B, C, D	C1
Ground	A, B, C, D	C1
First	A, B, C, D	C2
Second	A, B, C, D	C3

B4, B5 and B7 types), as well as to design the columns with the bigger side parallel to Y (and thus with the strong flexural axis parallel to X). The only beams with out-of-depth section in longitudinal direction are the B6 beams bearing the front staircase (frame alignment A). As shown in Fig. 5, the foundations are constituted by a mesh of inverse T-shaped RC beams. Their base sections are 2,310 mm-wide in Y direction and 1,450 mm-wide in X, with mutual 350 mm-high flanges, and 350 mm-high and 650 mm-wide webs in both directions.

Fig. 6 shows the nomenclature and locations of the perimeter infills and internal partitions situated on the three above-ground storeys, all made of clay brick masonry. The infills on the basement are the same as on the above-ground storeys; the partitions coincide with the ones of the ground storey, except for the longitudinal alignment, where the panels of the odd spans were removed and replaced by steel braces in 2005, as observed above. The geometrical and constructive characteristics of infills and partitions are recapitulated in Table 3, where symbols "Tr" and "Lo" mean that the elements are placed along the transversal and longitudinal directions, respectively. The double-layer infill types have intermediate cavities between the constituting layers varying from 50 to 150 mm, depending on the specific thermal insulation solution adopted for them.

A careful investigation campaign on materials and structural members, and dynamic identification tests on the building, had been carried out prior to designing the 2013 retrofit intervention. This campaign included on-site Son-Reb and pacometer analyses on beams and columns, and laboratory tests on concrete and steel bar samples extracted

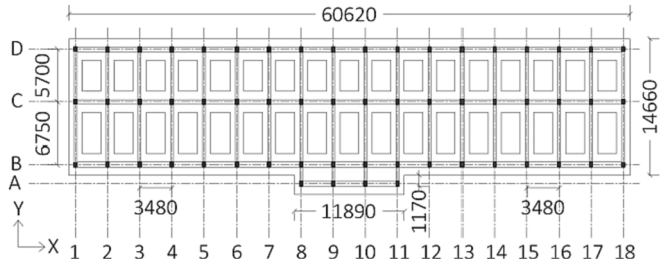

Fig. 5. Foundation plan (dimensions in mm).

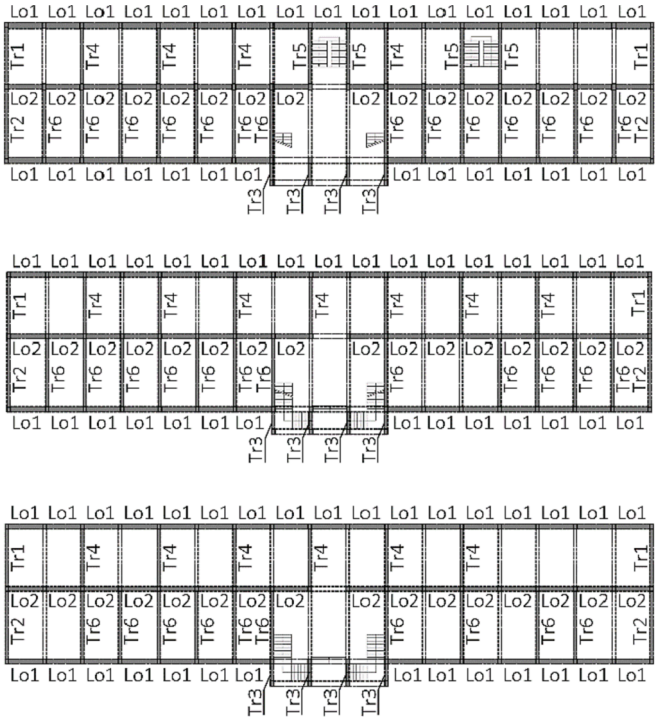

Fig. 6. Nomenclature and locations of infills and partitions (from top to bottom plan: ground, first and second storey).

from selected members. The following mechanical properties resulted from the experimental surveys: mean cubic compressive strength and Young modulus of concrete equal to 19.5 MPa and 22,000 MPa, respectively; yield stress and tensile strength of the steel bars equal to 315 MPa and 490 MPa, respectively. These were assumed as reference values for the finite element and stress check analyses, which are discussed in the next Section.

3. Seismic assessment analysis of the building

3.1. Structural model and modal analysis

As mentioned in the Introduction, the analysis is focused on the conditions preceding the 2013 retrofit intervention, which consisted in the installation of buckling restrained braces in several frame spans of the above-ground storeys. At the same time, the conventional steel braces installed on the basement storey in 2005 are kept unchanged in the assessment analysis. Indeed, they are considered as an integral part of the existing building, as assumed when the buckling restrained bracing system was designed. The finite element model of the structure, displayed in Fig. 7, was generated by the SAP2000NL calculus program [17]. Frame-type elements were assumed for the RC columns and beams. The presence of an external RC slab on the left portion of the rear façade of the building, and a RC slab covering the RC retaining walls in other zones of the building perimeter, both built during the 2005 intervention and structurally connected to the ground floor perimeter beams, were simulated in the finite element model with horizontal springs reproducing the in-plane stiffness of these slabs.

A modal analysis of the structure was initially carried out, which highlighted a first translational mode along X, with vibration period of 0.295 s and effective modal mass (EMM) equal to 75.4 %, and a first translational mode along Y, with period of 0.213 s and EMM of 74 %. Both periods are satisfactorily related to the experimental values surveyed by means of the above-mentioned dynamic identification tests carried out on the building before the incorporation of the buckling restrained braces [4]. Four, 18 and 52 modes are needed to activate

Table 3
Geometrical and constructive characteristics of perimeter infills and internal partitions.

Alignment	Characteristics
Tr1	Double-layer (120 mm-thick solid brick internal + 80 mm-thick vertically hollowed external) perimeter walls without openings
Tr2	Double-layer (120 mm-thick solid brick internal + 80 mm-thick vertically hollowed external) perimeter walls with openings
Tr3	Double-layer (120 mm-thick solid brick internal + 80 mm-thick vertically hollowed external) main entrance lateral walls
Tr4	Double-layer (80 mm + 80 mm-thick horizontally hollowed) classrooms and common areas partitions
Tr5	Double-layer (80 mm + 80 mm-thick horizontally hollowed) staircase partitions
Tr6	Single-layer (80 mm mm-thick horizontally hollowed) classrooms and common areas partitions
Lo1	Double-layer (120 mm-thick solid brick internal + 80 mm-thick vertically hollowed external) perimeter walls with openings
Lo2	Single-layer (80 mm mm-thick horizontally hollowed) classrooms and common areas partitions

summed modal masses greater than 85 % along X, Y, and around Z, respectively.

3.2. Time-history analysis – input accelerograms

The seismic assessment study was developed via time-history analysis by using as input the main shock components of the earthquake recorded by Norcia seismographic station on 30th October 2016. The elastic pseudo-acceleration response spectra at 5 % linear viscous damping ratio of the N-S, E-W and vertical component records are plotted in Fig. 8. According with the plan layout of the building, the N-S component was basically introduced in input along Y axis, and the E-W component along X. For the sake of completeness, different orientations were also considered for the two components by varying their incidence angle in plan. As a result of this enquiry, the highest seismic demand was determined by the N-S parallel to Y and E-W parallel to X basic input motion orientation.

3.3. Time-history analysis – finite element model of infills and partitions

As postulated in the Introduction, the structural model included also the substitute elements of masonry infills and partitions, which were typically built in contact with the RC frame elements. As is known, at the beginning of their seismic response, the undamaged cladding panels interact with the frame members, absorbing a portion of the horizontal action by means of their shear stiffness. Then, as seismic action increases, the panels tend to detach from the frame members along their span (beams) and height (columns), offering a residual collaboration to the dynamic response of the structure in the form of two crossed compression-resisting diagonal struts converging to the centre of the beam-to-column joints (one strut ascending from the lower left joint to the upper right joint, and vice versa for the other strut).

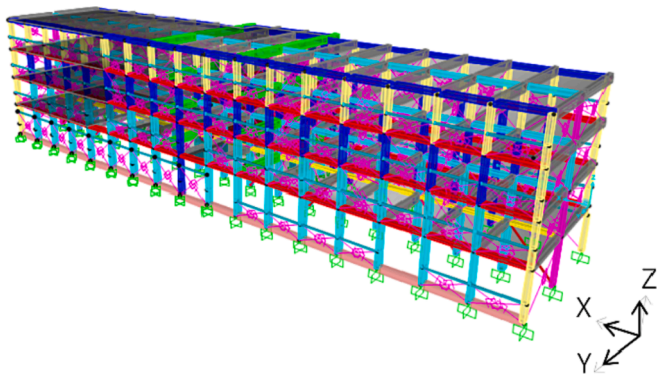

Fig. 7. Finite element model of the structure.

In the proposed numerical model, the behaviour of the struts is simulated by starting from the σ_s-ε_s axial stress-axial strain cyclic response curves and relevant peak envelope proposed by Crisafulli [18], schematically illustrated in Fig. 9a and Fig. 9b, respectively. Therein $\sigma_{s,\max}$ is the maximum stress surveyed in the strut, $\varepsilon_{s,abl}$ is the corresponding strain, and $E_{m\phi}$ is the Young modulus of the constituting masonry material evaluated in the direction parallel to the strut, defined by the inclination angle ϕ of the latter with respect to the horizontal axis. $E_{m\phi}$ can be estimated by the classical expression [19]:

$$E_{m\varnothing} = \left[\frac{cos^4\varnothing}{E_{mh}} + \frac{sin^4\varnothing}{E_{mv}} + cos^2\varnothing + sin^2\varnothing\left(\frac{1}{G} - \frac{\nu}{E_{mh}}\right)\right]^{-1} \quad (1)$$

where E_{mh}, E_{mv} are the Young moduli of masonry evaluated in horizontal and vertical direction, G is the shear modulus and ν is the Poisson ratio.

In order to pass from the σ-ε response of the material to the response of the panels, the b_s width of the equivalent strut must be evaluated first. This is done by means of the well-established relation [20]:

$$b_s = \left(\frac{K_1}{\lambda h_i} + K_2\right) d_s \quad (2)$$

where d_s = length of the strut, K_1, K_2 = empirical coefficients depending on the value of λh_i, as specified in Table 4, and λh_i = non-dimensional parameter, function of the geometrical and mechanical characteristics of the frame-infill (or frame-partition) system, with h_i = inter-storey frame height and λ expressed as [19]:

$$\lambda = \sqrt[4]{\frac{E_{m\phi}\, t_{mp} sin2\varnothing}{4E_c I_c h_{mp}}} \quad (3)$$

where t_{mp}, h_{mp} = thickness and height of the panel, E_c = Young

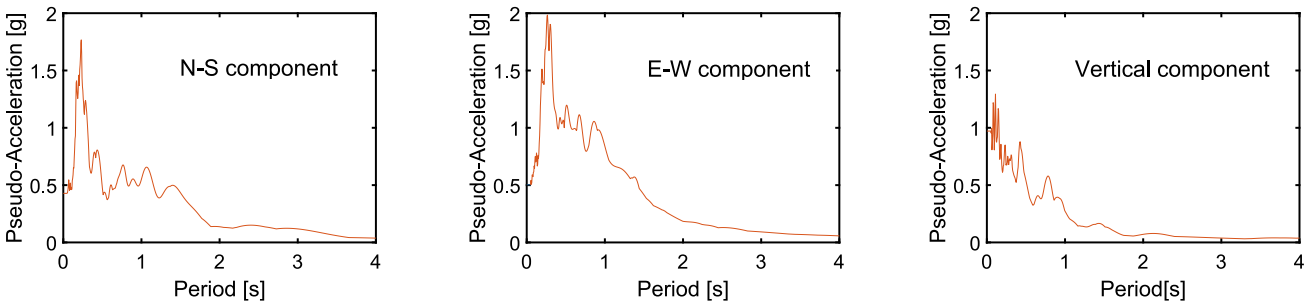

Fig. 8. Pseudo-acceleration elastic response spectra of 06:40:18, 30 October 2016 Norcia seismograph station records.

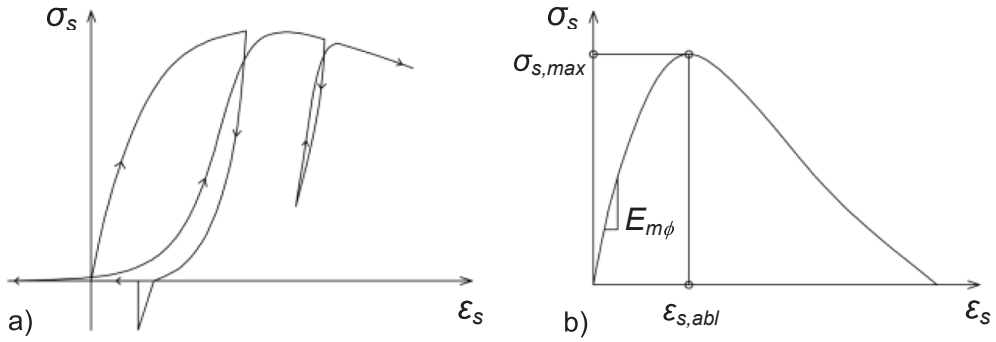

Fig. 9. a) Axial stress–axial strain cyclic response of the equivalent strut model; b) envelope of relevant peak values (adapted from [14]).

Table 4
K_1 and K_2 coefficient values.

	$\lambda h_i < 3.14$	$3.14 < \lambda h_i < 7.85$	$\lambda h_i > 7.85$
K_1	1.3	0.707	0.47
K_2	−0.178	0.01	0.04

modulus of the material constituting the columns adjacent to the infill (partition), and I_c = moment of inertia of the same columns calculated about the normal axis to the panel.

Similar to other recent research studies [5,21–26], a trilinear backbone scheme is assumed here to convert Crisafulli's σ-ε curve in the axial force (named H_s in the following)–axial displacement (D_s) curve of the strut. This curve is then transformed into the lateral force (H_p)– drift ratio (D_{pr}, i.e. the ratio of panel drift, D_p, to h_i) curve of the panel by which the performance of infills and partitions is assessed. To this aim, the peak strut force, $H_{s,\max}$, and peak panel force, $H_{p,\max}$, are computed by the following expressions [19]:

$$H_{s,max} = \sigma_{p,min} b_s t_s \tag{4}$$

$$H_{p,max} = \sigma_{p,min} b_s t_s cos\varnothing \tag{5}$$

where t_s is the thickness of the strut, coinciding with t_{mp}, $cos\phi$ is the geometrical factor needed to pass from $H_{s,\max}$ to $H_{p,\max}$ (as the strength of the panel is equal to the horizontal lateral strength of the strut), and $\sigma_{p,\min}$ is the minimum stress value associated with the achievement of one of the four possible failure mechanisms of the panel. These mechanisms are caused by: compression in the middle (σ_{p1}), compression at the corners (σ_{p2}), shear-sliding (σ_{p3}), and shear-diagonal crack (σ_{p4}), with σ_{p1}, σ_{p2}, σ_{p3}, and σ_{p4} evaluated as follows [20]:

$$\sigma_{p1} = \frac{1.16 f_{pv} tan\varnothing}{K_1 + K_2 \lambda h_i} \tag{6}$$

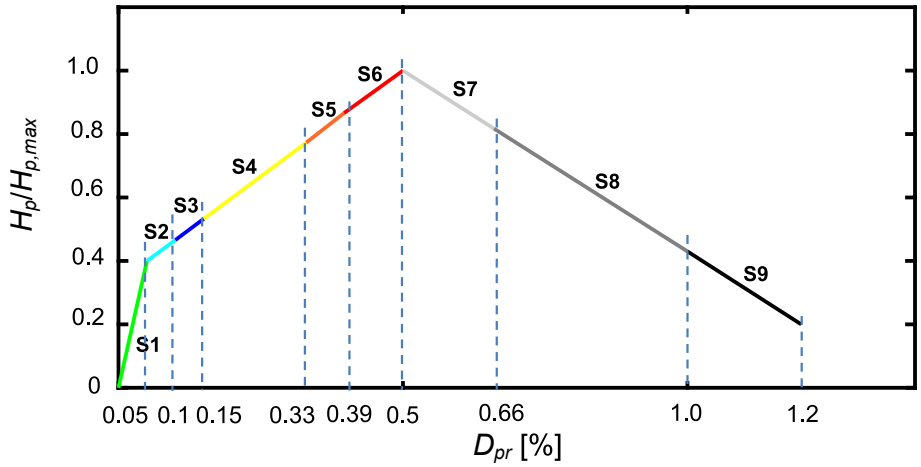

Fig. 10. Backbone curve for the analysis of infills and partitions graphed in terms of normalized lateral force of the panels.

$$\sigma_{p2} = \frac{1.12 f_{pv} sin\varnothing cos\varnothing}{K_1(\lambda h_i)^{-0.12} + K_2(\lambda h_i)^{0.88}} \tag{7}$$

$$\sigma_{p3} = \frac{(1.2 sin\varnothing + 0.45 cos\varnothing) f_{js} + 0.3\sigma_v}{b_s/d_s} \tag{8}$$

$$\sigma_{p4} = \frac{0.6 sin\varnothing f_{pd} + 0.3\sigma_v}{b_s/d_s} \tag{9}$$

In expressions (6) through (9) f_{pv} is the compressive strength of the panel, f_{js} the sliding resistance of the mortar joints, f_{pd} is the shear resistance of the panel under diagonal compression, and σ_v is the vertical compression stress, null for panels without load-bearing function with respect to vertical loads (like the infills and partitions of the case study building).

The relation between the ε_s axial strain of the strut and D_{pr} is given by the following geometrical transformation:

$$D_{pr} = l_i - \sqrt{d_s{}^2(1-\varepsilon_s)^2 - h_i{}^2} \tag{10}$$

with l_i = centerline length of the frame span where the panel is included.

Based on the evaluation of $H_{p,\max}$ and D_{pr} by means of expressions (5) and (10), the construction of the trilinear backbone H_p–D_{pr} curve is carried out by a phenomenological approach, collecting and elaborating several experimental and numerical modelling/assessment literature data. The resulting curve is traced out in Fig. 10, where D_{pr} is expressed in percent unit, and H_p is normalized to $H_{p,\max}$, so as to obtain a non-dimensional notation for the lateral force too. The curve is divided into nine segments, named S1 through S9 in Fig. 10, scanned by means of eight D_{pr} performance limit values, as summarized below.

The first response segment (S1, traced out in green) corresponds to a non-cracked linear-elastic behaviour of the panel, whose limit can be approximately fixed at a D_{pr} value of 0.05 % [27]. The corresponding $H_p/H_{p,\max}$ value, which represents the cracking lateral force of the panel, H_{cr}, is assumed to be equal to 0.4, according with the suggestions offered in [22–23,28]. A first set of diffused hairline and visible fissures (with maximum width of about 1 mm) starts at the end of S1, causing a loss of lateral stiffness and the beginning of the cracked response stage [29]. More appreciable surface cracks are displayed in the S2 (light blue) branch, inducing more accentuated plaster damage, with maximum crack width no greater than 2 mm, and D_{pr} limit value of 0.1 % [24,28]. A wider manifestation of surface cracks occurs in branch S3 (dark blue), with crack width reaching about 3 mm and more visible plaster damage, up to a drift ratio of 0.15 % [24]. In depth cracking effects begin to develop along S4 branch (yellow) [24–25], whose D_{pr} threshold can be located at 0.33 %. This value is also normally assumed by seismic Standards as the limit identifying the Operational (OP) performance level for frame buildings in the presence of masonry infills and partitions [30–31]. Branch S5 (orange) identifies the response stage where the lateral sides of the panel start to detach from the adjacent columns and the upper side from the top beams. Beginning from the S5 limit, which can be fixed at 0.4 % [24–25], segment S6 (red) marks the first level of damage triggering the development of the prevailing failure mechanism, among the four ones described by relations (5) through (8). The drift ratio limit of this branch coincides with the attainment of $H_{p,\max}$, and is assessed by most seismic Standards as the threshold of the Immediate Occupancy performance level [30–31]. This implicitly corresponds to a "repairable" damage condition, not impairing the usage of the building but requiring in-depth post-quake restoration interventions of the panels. For standard hollow clay brick masonry typical of the 1960 s, with hole percent area (i.e. the percent ratio of the area of the holes to the cross section area of the bricks) greater than 55 %, the Immediate Occupancy drift limit is normally put as equal to 0.5 % [30]. The negative slope of the softening branch following the attainment of $H_{p,\max}$ can be identified by an angle of about 30°, by averaging data in [22–26].

The first segment of the softening branch, S7 (light grey), corresponds to the development of damage effects related to the prevailing possible failure mechanism, with appreciable cracking throughout the brick units, their local crushing and spalling, as well as sliding in mortar joints.

The transition to the second descending branch (S8, dark grey) can be located at a drift ratio of about 0.66 %. The S8 segment defines a range of severe-to-very severe—and substantially irreparable—damage of clay brick infills and partitions (i.e. a damage level for which their possible reparation cost would exceed their complete demolition and reconstruction cost). The end of S8 segment is fixed at a point of coordinates $H_p/H_{p,\max} = 0.35$ [21] and $D_{pr} = 1$ % [23–24]. This point can be assumed to coincide with, or to be slightly lower than, the attainment of the Life Safety performance level limit, as it implies local falling of masonry units or small panel portions, normally not threatening for the building occupants, and thus without direct risks of life losses. Small residual response capacities of panels exist up to a lateral force value, H_r, equal to $0.2H_{p,\max}$, to which a drift ratio approximately equal to 1.2 % corresponds (S9 branch, black). Beyond this limit, full collapse of infills and partitions normally occurs, most often in their plane, consistently with one of the four mechanisms discussed above, or a combination of some of them. A final overturning of panels—or their significant portions—can sometimes be observed, which is induced by the orthogonal seismic response component, as the last step of a degradation process mainly related to the in-plane damage.

The interaction between in-plane and out-of-plane response of masonry infills was investigated in recent studies [32–34], offering effective criteria and procedures for their nonlinear computational modelling. This interaction was not included in the analysis of the case study building because only an infill panel situated on the upper storey showed an out-of-plane near collapse condition, following the development and propagation of severe in-plane cracks.

The presence of doors and windows in infills and partitions is taken into account by computing the strength and stiffness contribution of the vertical portions of the panels net of the openings [23,26].

By way of example of the resulting non-normalized H_p–D_{pr} backbone curves for the 193 panels modelled in the analyses, Fig. 11 shows the ones concerning the main elements without openings, belonging to the following types: Tr1 (double-layer, 120 mm-thick solid brick internal + 80 mm-thick vertically hollowed perimeter panels, with $l_i = 5$ m, for which: $H_{p,cr} = 68.9$ kN, $H_{p,\max} = 172.5$ kN, $H_{p,r} = 34.5$ kN); Tr4 (double-layer, 80 mm + 80 mm-thick horizontally hollowed partition panels, with $l_i = 5$ m, and $H_{p,cr} = 41.6$ kN, $H_{p,\max} = 104$ kN, $H_{p,r} = 20.8$ kN); Tr6 (single-layer, 80 mm mm-thick horizontally hollowed partition panels, with $l_i = 6.1$ m, and $H_{p,cr} = 27.3$ kN, $H_{p,\max} = 68.3$ kN, $H_{p,r} = 13.7$ kN); Lo2 (single-layer, 80 mm-thick horizontally hollowed partition panels, with $l_i = 3.5$ m, and $H_{p,cr} = 14.1$ kN, $H_{p,\max} = 35.3$ kN, $H_{p,r} = 7.1$ kN).

The hysteretic behaviour of the panels is reproduced by means of the

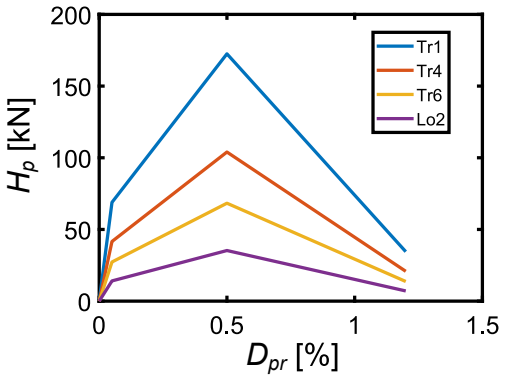

Fig. 11. Backbone curves for Tr1, Tr4, Tr6 and Lo2-type panels without openings.

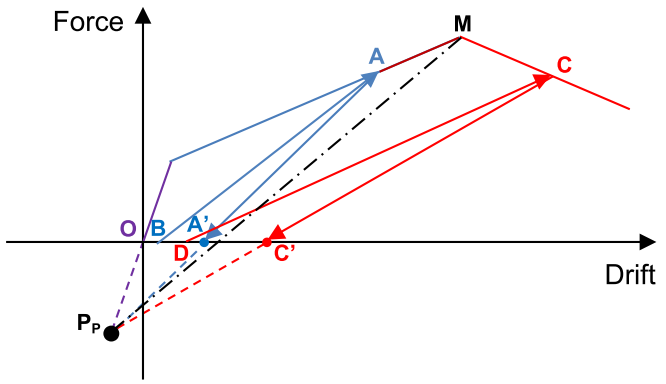

Fig. 12. Multi-linear no-tension pivot model adopted to simulate the hysteretic response of infills and partitions.

multilinear no-tension pivot-type rule schematized in Fig. 12. As illustrated by this graph, starting from any point of the backbone curve (e.g., points A, C situated on the second and third branch, respectively), the unloading lines converge to a mutual pivot point, P_p. This is fixed as the intersection of the elastic branch, prolonged in the tensile quadrant of the drift-force diagram, with the dashed-dotted line passing from the maximum response point, M, having a slope equal to half of the elastic branch stiffness. The points which the reloading lines start from (B, D in the demonstrative graph) are located at a predetermined fraction *f* of the segments determined on the horizontal axis by the intersections with the unloading lines (i.e., segment OB is *f* times OA', and segment OD is *f* times OC'). Each reloading line converges to the maximum loading point reached in the previous cycle (thus, determining the reloading segments BA and DC in the graph). The *f* stiffness degradation parameter ranges from 0 (null degradation, in which case the reloading lines follow the unloading ones) to 1 (maximum degradation, in which case the reloading lines are the secants joining the origin to the unloading points). By referring to several literature suggestions [21–22,25–26], *f* was basically put as equal to 0.7 in the analyses developed in this study. Different *f* values were also assumed for the sake of completeness, included in the (0.5–0.8) range, showing a marginal influence on results.

The additional no-tension rule applied to the hysteretic pivot model prevents the force from inverting its sign, thus limiting the unloading lines to zero force values.

3.4. Time-history analysis –results

The results of the analysis for the structural members highlight 75 % of columns and 62 % of beams in unsafe conditions. By way of example of these results, the biaxial moment interaction curves—where M_1, M_2 are the bending moments around the two local reference axes of the element cross sections—for the ground, first and second storey columns belonging to the B/8 alignment (where the grid line is denoted by the letter and the number deduced from Fig. 2) are plotted in Fig. 13. These curves remarkably overcome the boundaries of the axial force-biaxial moment safe domains, traced out for comparison, on all storeys, reaching maximum values of the demand/capacity ratio equal to about 2.2 (ground storey), 1.8 (first) and 1.35 (second). Like for all remaining alignments, the basement columns are in safe conditions because this storey is nearly blocked to the horizontal translation along both axes in plan by the above-mentioned RC slabs connecting a wide portion of the perimeter cavity wall, in addition to the traditional steel braces installed in 2005.

Concerning partitions and infills, the lateral force-drift ratio response cycles of the ground, first and second storey Lo2-type partition panels situated between C/6 and C/7 column alignments, and first storey Tr2-type infill panels located between B/18 and C/18 column alignments are displayed in Figs. 13 and 14, respectively. These graphs, all referred to the analyses carried out with the above-mentioned $f = 0.7$ value, show the combined response of the two struts constituting the panels, where the positive sign of drifts and forces is consistent with the positive direction of the reference X and Y axes. Fig. 14 highlights the achievement of drift ratios equal to 1.02 % (black branch of the backbone curve, beyond the Life Safety limit and identifying irreparable damage conditions) for the ground storey, 0.9 % (black branch, irreparable damage) for the first, and 0.67 % (beginning of the dark grey branch, severe damage) for the second. The response of the Tr2-type infill in Fig. 15 reaches a drift ratio of 0.85 %, denoting irreparable damage too. A photographic image of the ground storey Lo 2-type partition dealt with in Fig. 14 is displayed in Fig. 16, highlighting a remarkable correlation with the irreparable damage conditions identified via numerical analysis.

In 82 % of partitions and infills the governing response mechanism resulted to be shear-diagonal crack, identified by the σ_{p4} ultimate stress; the shear-sliding mechanism (σ_{p3}) was observed for the remaining panels, all of which of under-window type. In order to synthesize the overall performance of the panels, colour maps assessing their post-quake state according with the chromatic scale of the backbone curve are plotted in Fig. 17 (longitudinal alignments) and 18 (transversal alignments). By collecting the data visualized in these drawings, the following damage state classification of panels is deduced, expressed in percent fractions of the total number of panels in X (198) and Y (88), by referring to the backbone curve branch nomenclature: S1 – 4.5 % (X), 0 (Y); S2 – 0.6 % (X), 14.8 % (Y); S3 – 7.6 % (X), 8 % (Y); S4 – 18.7 % (X), 13.6 % (Y); S5 – 16.5 % (X), 33 % (Y); S6 – 24.7 % (X), 19.3 % (Y); S7 – 1 % (X), 1.2 % (Y); S8 – 25.8 % (X), 9.1 % (Y); S9 – 0.6 % (X), 0 (Y). By summing up, 18.7 % of panels in X and 13.6 % in Y suffer a light damage (S4), 41.2 % in X and 52.3 % in Y a moderate damage (S5-S6), 1 % in X and 1.2 % in Y a moderate-to-severe damage (S7), 25.8 % in X and 11.2 % in Y a severe-to-very severe and irreparable damage (S8), and 0.6 % in X a near-full collapse damage. These results confirm that, as highlighted by the post-quake field surveys, the incorporation of the buckling restrained braces did not guarantee a satisfactory protection of partitions and infills. As premised in the Introduction, this suggested to evaluate a different supplemental damping-based retrofit strategy

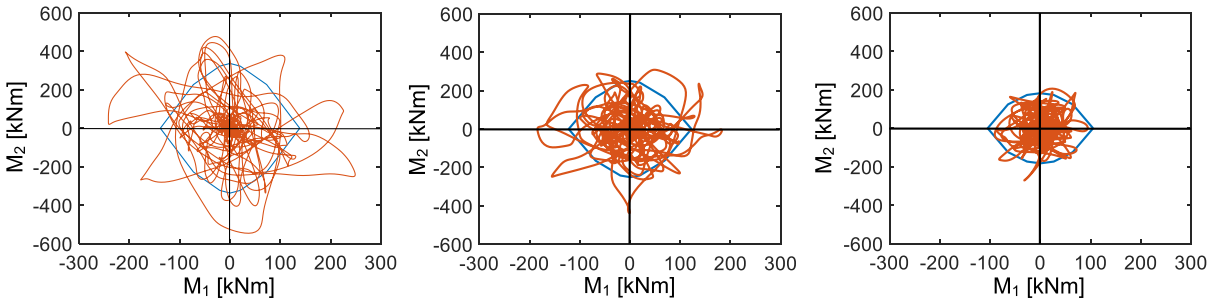

Fig. 13. Biaxial moment curves for B/8 column alignment (from left to right: ground, first and second storey).

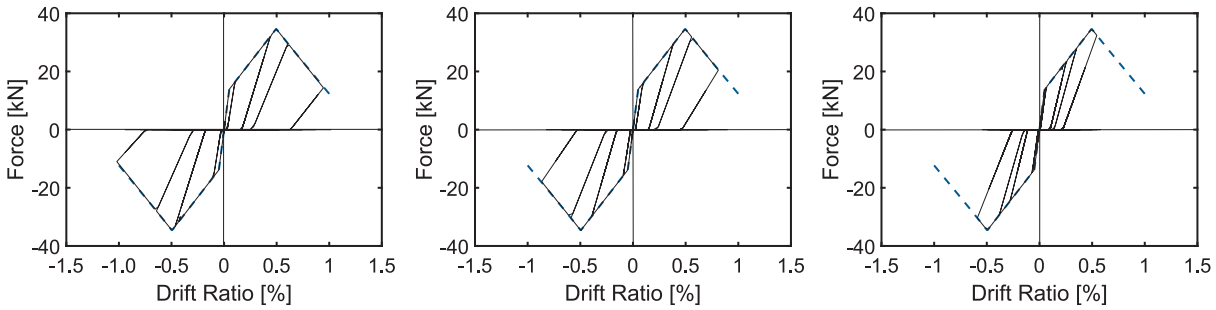

Fig. 14. Response cycles of Lo2-type partition panels situated in the C/6-C/7 frame spans (from left to right: ground, first and second storey).

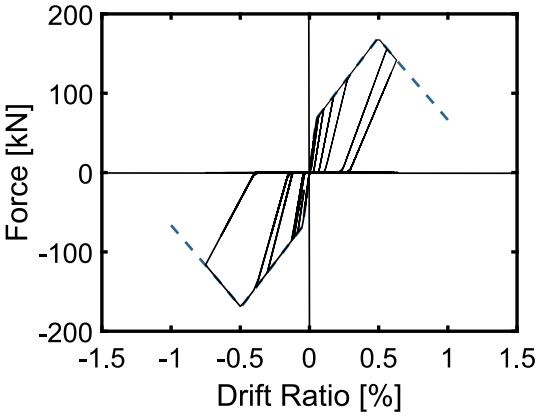

Fig. 15. Response cycles of Tr2-type infill panel situated in the B/18-C/18 span on first storey.

Fig. 16. Image of Lo2-type partition panel situated in the C/6-C/7 span on ground storey taken after 30th October 2016 earthquake.

starting from the pre-existing conditions of the building, as discussed in the following Section.

4. Alternative dissipative bracing-based retrofit hypothesis

The intervention hypothesis consists in the installation of a dissipative bracing system incorporating PFV spring-dampers along both directions in plan, and namely in the following twelve frame spans on the three above-ground storeys: B/6–B/7, B/11–B/12, B/12–B/13, D/6–D/7, D/11–D/12, D/12–D/13 in X; and C/1–D/1, C/3–D/3, C/5–D/5, C/11–D/11, C/13–D/13, C/18–D/18 in Y. A view of the finite element model including the protection system is shown in Fig. 19.

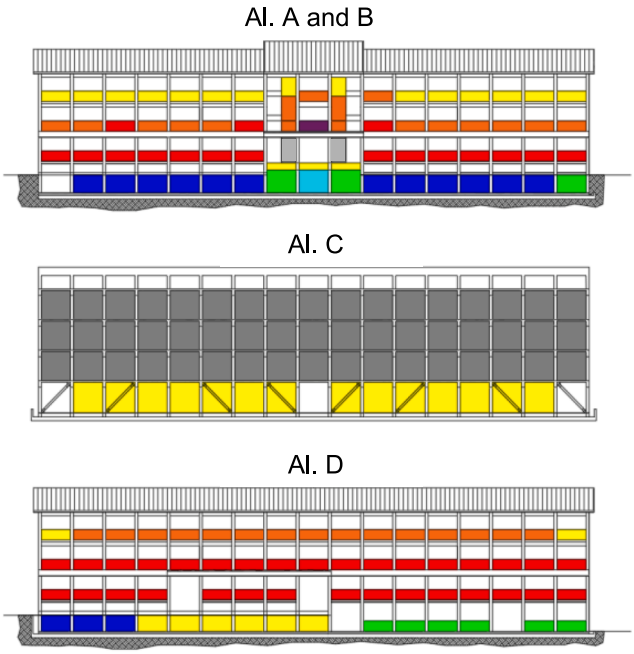

Fig. 17. Colour representation of the post-quake state of panels in X direction according to the chromatic scale of the backbone curve.

According with the general layout of the protective system adopted for frame structures [11–13], and as illustrated by the installation detail reproduced in Fig. 19, the PFV devices are mounted in pairs at the tip of the supporting inverted V-shaped steel trusses. A half-stroke initial position is imposed to their pistons, so as to obtain a symmetric tension–compression response capacity. Due to the in-series dampers-to-trusses connection, the low stiffness of the PFV dissipaters causes a little increase of the lateral stiffness of the structure, which represents an effective property when prevailing supplemental damping over stiffening effects are targeted in the conception of a dissipative bracing technology.

The mechanical behaviour of the PFV devices is characterized by the following damping force, F_d, and elastic force, F_e, components [35–37]:

$$F_D(t) = c\,\mathrm{sgn}[\dot{x}(t)]|\dot{x}(t)|^{\gamma} \tag{11}$$

$$F_e(t) = \frac{(k_1 - k_2)x(t)}{\left[1 + \left|\frac{k_1 x(t)}{F_0}\right|^5\right]^{1/5}} \tag{12}$$

where: t = time variable; c = damping coefficient; $sgn(\cdot)$ = signum function; $\dot{x}(t)$ = velocity; $|\cdot|$ absolute value: γ = fractional exponent, ranging from 0.1 to 0.2; F_0 = static pre-load; k_1, k_2 = stiffness of the

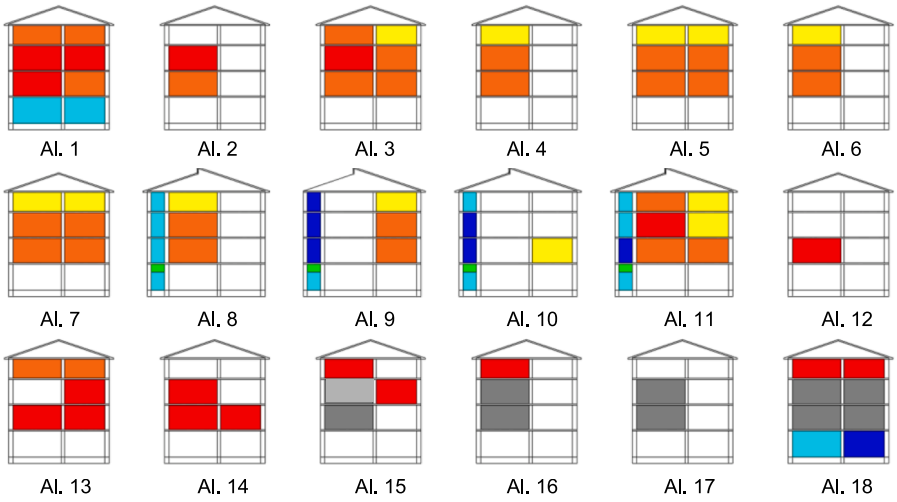

Fig. 18. Colour representation of the post-quake state of panels in Y direction according to the chromatic scale of the backbone curve.

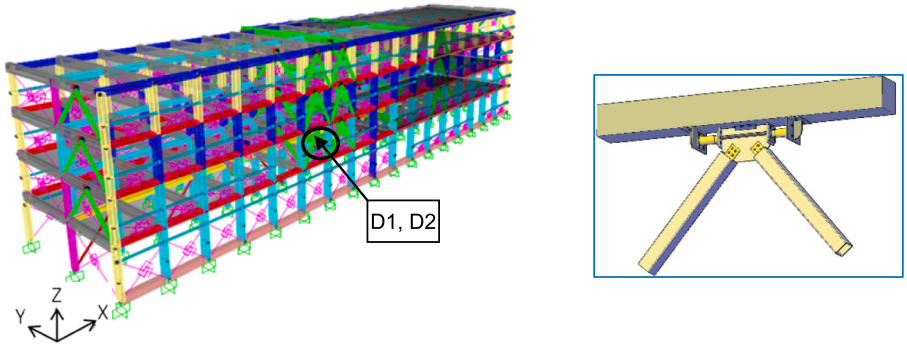

Fig. 19. Finite element model of the structure including the dissipative bracing system, and installation detail of a pair of PFV spring-dampers.

response branches situated below and beyond F_0; and $x(t)$ = displacement.

The spring-dampers were designed by referring to the energy-based criterion proposed by the first and third author in [11], which consists in assigning them the capability of dissipating, on each storey, a prefixed energy fraction, $E_{d,t}$, of the seismic input energy, $E_{i,t}$, transmitted to the structure on that storey. $E_{i,t}$ is calculated for the real ground motion adopted in the analyses, like in this case, or a pre-fixed normative earthquake level. As basically assumed in retrofit designs of RC frame structures [12–13,16], in this application $E_{d,t}$ was fixed at 80 % of $E_{i,t}$. The following $E_{d,t}$ demands derive from this hypothesis for the three storeys and the two directions in plan: 230.4 kJ (ground storey), 280.8 kJ (first), 201.6 kJ (second) in X; and 227.2 kJ (ground), 296.4 kJ (first), 234 kJ (second) in Y. The corresponding energy demands on each dissipater, $E_{d,sd} = E_{d,t}/12$, descend: 19.2 kJ (ground storey), 23.4 kJ (first), 16.8 kJ (second) in X; and 20.6 kJ (ground), 24.7 kJ (first), 19.5 kJ (second) in Y. The maximum $E_{d,sd}$ demands in the two directions, both computed for the first storey, are met by a PFV spring-damper in current production [37] with nominal energy dissipation capacity, E_n, equal to 25 kJ. Since E_n of the immediately smaller standard spring-damper type is equal to 16.5 kJ, i.e. capable of approximately meeting only the second storey energy demand in X, it was assumed to install the devices with $E_n = 25$ kJ capacity on all storeys in both directions. The remaining mechanical properties of the selected type of device are as follows: c =

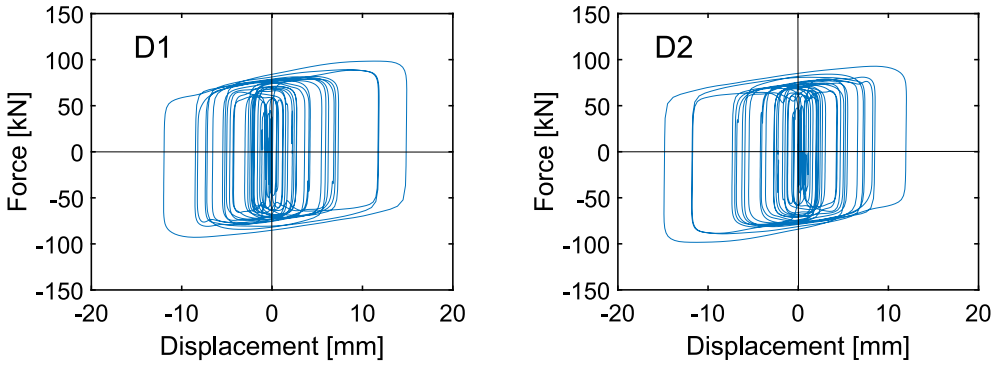

Fig. 20. Response cycles of the D1, D2 spring-damper pair highlighted in Fig. 18.

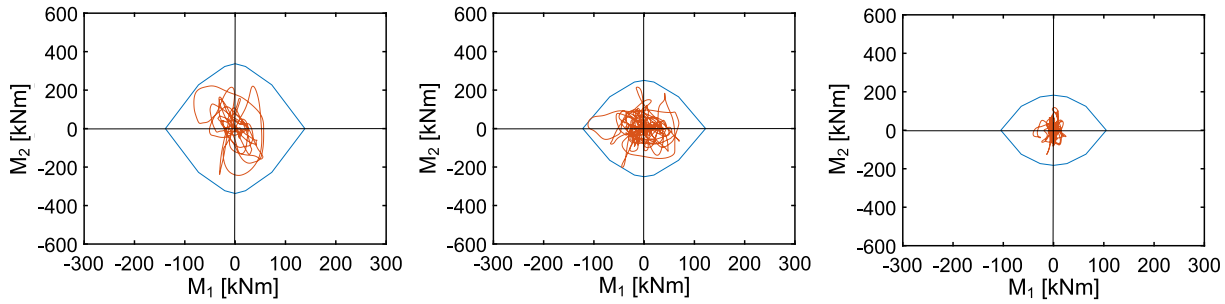

Fig. 21. Biaxial moment curves for B8 column alignment (from left to right: ground, first and second storey) – retrofitted conditions.

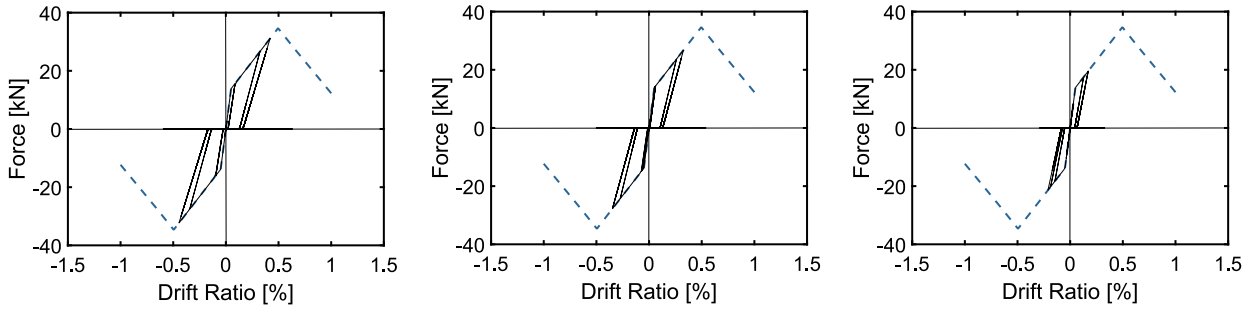

Fig. 22. Response cycles of Lo2-type partition panels situated between C6 and C7 column alignments (from left to right: ground, first and second storey) – retrofitted conditions.

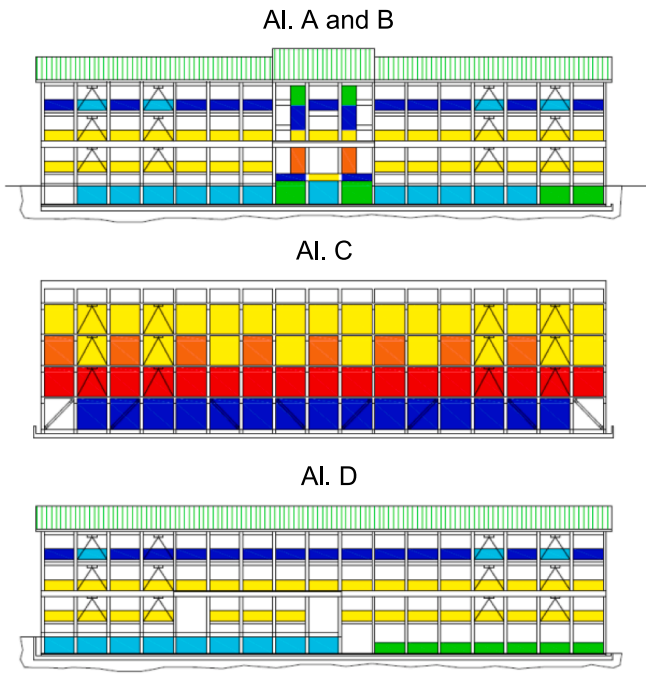

Fig. 23. Colour representation of the response state of panels in X direction according to the chromatic scale of the backbone curve – retrofitted conditions.

38 kN·(s/mm)$^{\gamma}$, $\gamma = 0{,}15$, $F_0 = 60$ kN, $k_2 = 1{,}55$ kN/mm, stroke $s_{max} = \pm$ 50 mm.

As expected, the modal parameters are scarcely influenced by the installation of the protective system, showing reductions of the fundamental periods by 3.3 % in X (from 0.295 s to 0.285 s) and 2.9 % in Y (from 0.213 s to 0.207 s), and negligible differences on relevant effective masses, as well as on the remaining modes.

By way of example of the spring-dampers performance, the response cycles of the D1, D2 pair of devices highlighted in the finite element model view of Fig. 19 are plotted in Fig. 20. As visualized by these graphs, maximum displacements of 16.5 mm are reached, i.e. equal to about one third of the stroke capacity; furthermore, an initial activation force of about 50 kN is shown, which was reached in correspondence with the attainment of a peak input acceleration of about 0.08 g. This value is 2.5 times smaller than the above-mentioned estimated peak of 0.2 g when the buckling restrained braces started to respond during the 2016 earthquake.

The building performance improvement in retrofitted conditions is synthesized by the graphs in Figs. 21-22 and drawings in Figs. 23-24, which duplicate the graphs in Figs. 13-14 and the drawings in Figs. 17-18 commented above in original state. The biaxial moment interaction curves of columns belonging to the B/8 alignment, shown in Fig. 21, are constrained within relevant safe domains. The same occurs for all remaining columns, with reduction factors in the stress states reaching maximum values of 2.5 as compared to the pre-retrofit conditions. The response of all beams too, not detailed here for brevity's sake, reaches safe conditions, both in terms of bending moment and shear.

The peak drift ratios of the partition panels in Fig. 22 are below the 0.33 % Operational performance level limit, for the first and second storey, and the 0.5 % Immediate Occupancy-related limit, for the ground storey. More specifically, they are equal to about 0.45 % on ground storey (S6 branch of the backbone curve, moderate damage), 0.32 % on first storey (terminal zone of S4 branch, light damage) and 0.18 % on second storey (beginning of S4 branch, very light damage). By considering that—storey by storey—these panels are subjected to the highest drift demands, their response assesses a substantial performance enhancement of the non-structural elements, in addition to the frame members, with marginal repair works and related costs for a small number of partitions and infills. This is confirmed by the damage colour maps in Figs. 23 and 24, which show that in longitudinal direction only the ground storey partitions (8.5 % of the total number of panels) reach the S6 response branch, and ten partitions plus two infills (4.9 %) the S5 branch. The response of the remaining panels is restrained to S1 (17.2 %), S2 (10.6 %), S3 (18.7 %) and S4 (40.2 %). In transversal direction,

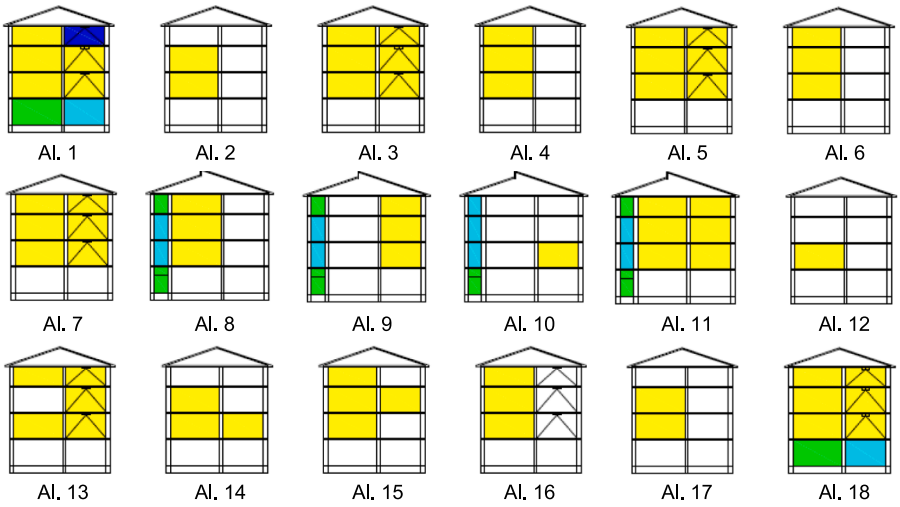

Fig. 24. Colour representation of the response state of panels in Y direction according to the chromatic scale of the backbone curve – retrofitted conditions.

the response does not exceed S4 for all panels, with 10.2 % of elements in S1, 12.4 % in S2, 1.2 % in S3 and 76.2 % in S4.

5. Conclusions

Protection of masonry partitions and infills, in addition to structural members, is a basic objective of retrofit interventions on frame structures where they have been originally built in contact—and thus seismically interacting—with the surrounding beams and columns.

Dissipative bracing technologies help meeting this goal by remarkably reducing both inter-storey drifts (which partitions and infills are sensitive to) and shears (a significant portion of which is absorbed by these panels by means of their well-known equivalent strut response mechanism). However, a prompt activation of the supplemental damping contribution offered by dissipative technologies is needed to avoid an initial "unprotected" transient response stage, during which remarkable damage can occur in non-structural elements.

This circumstance was experienced by the Italian school building examined in this article, where the buckling restrained bracing system installed in 2013 began to respond from an input acceleration of about 0.2 g during the October 30, 2016 earthquake, as estimated in assessment studies carried out by other authors.

The alternative dissipative bracing-based retrofit hypothesis proposed here, designed by referring to the pre-2013 conditions of the building, produced a remarkable seismic performance improvement, thanks to the high damping capacity of the constituting PFV spring-dampers and their activation from the early seismic response stages (i.e. in correspondence with a peak input acceleration of about 0.08 g).

More detailed remarks derived from the results of the study are summarized below.

- In order to carefully check the response of partitions and infills in non-linear time-history analyses, a trilinear axial force–axial displacement backbone curve was generated for their equivalent strut elements and transformed in the lateral force–drift curve of the panels. The latter was divided into nine sub-branches, the limits of which were fixed by referring to the results of several literature studies on representative specimens and models. Although these limits could be calibrated further for specific types of masonry infills and partitions, by complying with corresponding experimental and numerical research data, they helped to quantitatively estimate the damage states of the case study building panels, and can become a useful reference for assessment studies of other buildings with similar cladding panels.
- A notable correlation with the post-quake damage conditions of partitions and infills emerged from the analyses carried out in the original state of the building. This confirmed that the buckling restrained braces did not appreciably protect the panels. On the other hand, they guaranteed an acceptable level of protection to the frame structure, which suffered limited plasticizations of beams and columns, as assessed by literature assessment studies, as well as by the post-quake field surveys.
- In current state, 75 % of columns and 62 % of beams are in unsafe conditions; at the same time, moderate-to-severe damage is evaluated for more than 40 % of panels in X and 50 % in Y, and very severe and irreparable damage for more than 25 % of panels in X and 10 % in Y.
- In retrofitted conditions, reduction factors in the stress states of columns and beams up to 2.5 are obtained, which allows attaining safe conditions in all structural members. The response of panels is restrained below the Operational performance level limit, except for about 13 % of elements in X for which the response is below the Immediate Occupancy limit, with at most a light damage level.
- The dissipative bracing system incorporating the PFV spring-dampers produces small stiffening effects on the frame structure, as it works primarily on the addition of supplemental damping capacity. This generates small increase of axial force in columns, as well as of flexural and shear stress states in the foundations, during seismic response, not requiring strengthening interventions either on the former or the latter.

CRediT authorship contribution statement

Stefano Sorace: Conceptualization, Methodology, Validation, Writing – review & editing, Supervision, Funding acquisition. **Iacopo Costoli:** Software, Validation, Investigation, Data curation. **Gloria Terenzi:** Conceptualization, Methodology, Validation, Visualization, Supervision, Funding acquisition.

Declaration of Competing Interest

The authors declare that they have no known competing financial interests or personal relationships that could have appeared to influence the work reported in this paper.

Data availability

Data will be made available on request.

Acknowledgements

The study reported in this paper was sponsored by the Italian Department of Civil Protection within the ReLUIS-DPC Project 2022/2024, WP 15 “Normative contributions on seismic Isolation and Dissipation”. The authors gratefully acknowledge this financial support.

References

[1] Di Ludovico M, Digrisolo A, Moroni C, Graziotti F, Manfredi V, Prota A, et al. Remarks on damage and response of school buildings after the Central Italy earthquake sequence. Bull Earthq Eng 2018;17:5679–700.
[2] Mazzoni S, Castori G, Galasso C, Calvi P, Dreyer R, Fischer E, et al. 2016–2017 Central Italy earthquake sequence: Seismic retrofit policy and effectiveness. Earthq Spectra 2018;34(4):1671–91.
[3] Fiorentino G, Nuti C, Paolacci F. Seismic response to 2016 Central Italy earthquakes of BRB retrofitted school building in Norcia. In: Proceedings of the 16th World Conference on Earthquake Engineering, 16WCEE. Santiago, Chile; 2017, Paper 5010.
[4] Lima C, et al (25 authors). Nonlinear modeling approaches for existing reinforced concrete buildings: the case study of De Gasperi-Battaglia school building in Norcia. In: Proceedings of the Italian Concrete Days 2018, Milan/Lecco, Italy; 2018. Lecture Notes in Civil Engineering Book Series 2020; 42: 82–95, Springer.
[5] Mazza F, Donnici A. In-plane and out-of-plane seismic damage of masonry infills in existing r.c. structures: the case study of De Gasperi-Battaglia school in Norcia. Bull Earthq Eng 2021;19(1):345–76.
[6] Foti D. Response of frames seismically protected with passive systems in near-field areas. Int J Struct Eng 2014;5:326–45.
[7] Foti D, Bozzo LM, Lopez-Almansa F. Numerical efficiency assessment of energy dissipators for seismic protection of buildings. Earthq Eng Struct Dyn 1998;27:543–56.
[8] Kavyashree BG, Patil S, Rao VS. Review on vibration control in tall buildings: from the perspective of devices and applications. Int J Dynam Control 2021;9(3):1316–31.
[9] Mazza F, Vulcano A. Displacement-based design procedure of damped braces for the seismic retrofitting of r.c. framed buildings. Bull Earthq Eng 2015;13:2121–43.
[10] Nuzzo I, Losanno D, Caterino N. Seismic design and retrofit of frame structures with hysteretic dampers: a simplified displacement-based procedure. Bull Earthq Eng 2019;17:2787–819.
[11] Sorace S, Terenzi G. Seismic protection of frame structures by fluid viscous damped braces. ASCE J Struct Eng 2008;134(1):45–55.
[12] Sorace S, Terenzi G, Fadi F. Shaking table and numerical seismic performance evaluation of a fluid viscous-dissipative bracing system. Earthq Spectra 2012;28:1619–42.
[13] Sorace S, Terenzi G, Bertino G. Viscous dissipative, ductility-based and elastic bracing design solutions for an indoor sports steel building. Adv Steel Constr 2012;8:295–316.
[14] Mori C, Sorace S, Terenzi G. Seismic assessment and retrofit of two heritage-listed R/C elevated water storage tanks. Soil Dyn Earthq Eng 2015;77:123–36.
[15] Licari M, Sorace S, Terenzi G. Nonlinear modeling and mitigation of seismic pounding between R/C frame buildings. J Earthq Eng 2015;19:431–60.
[16] Terenzi G, Costoli I, Sorace S. Activation control extension of a design method of fluid viscous dissipative bracing systems. Bull Earthq Eng 2020;18(8):4017–38.
[17] CSI. SAP2000NL. Theoretical and user’s manual. Release 23.04. Computers & Structures Inc., Berkeley, CA, USA, 2022.
[18] Crisafulli FJ. Seismic behaviour of reinforced concrete structures with masonry infills. PhD Thesis, University of Canterbury, Christchurch, New Zealand, 1997.
[19] Stafford SB. Behaviour of square infilled frames. ASCE J Struct Division 1966;92(1):381–403.
[20] Bertholdi SH, Decanini LD, Gavarini C. Telai tamponati soggetti ad azione sismica, un modello semplificato: confronto sperimentale e numerico. In: Proceedings of the VI Italian National Conference on Earthquake Engineering, 1993, 2:815–824 (in Italian).
[21] Crisafulli FJ, Carr AJ, Park R. Analytical modelling of infilled frame structures—a general overview. Bull New Zealand Soc Earthq Eng 2000;33(1):30–47.
[22] Cavaleri L, Di Trapani F. Cyclic response of masonry infilled RC frames: experimental results and simplified modelling. Soil Dyn Earthq Eng 2014;65:224–42.
[23] Noh NM, Liberatore L, Mollaioli F, Tesfamariam S. Modelling of masonry infilled RC frames subjected to cyclic loads: State of the art review and modelling with OpenSees. Eng Struct 2017;150:599–621.
[24] Morandi P, Hak S, Magenes G. Performance-based interpretation of in-plane cyclic tests on RC frames with strong masonry infills. Eng Struct 2018;156:503–22.
[25] Gaetani d’Aragona M, Polese M, Prota A. Effect of masonry infill constitutive law on the global response of infilled RC buildings. Buildings 2021;11: article 57:25 pp.
[26] Mucedero G, Perrone D, Brunesi E, Monteiro R. Numerical modelling and validation of the response of masonry infilled RC frames using experimental testing results. Buildings 2021; 10:182, 30 pp.
[27] Mazza F, Donnici A. In-plane-out-of-plane single and mutual interaction of masonry infills in the nonlinear seismic analysis of RC framed structure. Engineering Structures 2022; 257:114076, 18 pp.
[28] Graziotti F, Penna A, Magenes G. A comprehensive in situ and laboratory testing programme supporting seismic risk analysis of URM buildings subjected to induced earthquakes. Bull Earthq Eng 2019;17:4575–99.
[29] Parisse F, et al (20 authors). Benchmarking the seismic assessment of unreinforced masonry buildings from a blind prediction test. Structures 2021; 31:982–1005.
[30] Decree M. Update of Technical Standards for construction”. Italian Ministry of Infrastructure and Transport 17 January 2018.. Rome, Italy, 2018 (in Italian.
[31] Eurocode 8, “Design of structures for earthquake resistance – Part 1: General rules, seismic actions and rules for buildings,” The European Union, Directive 2004/18/EC, Brussels, Belgium, 2004.
[32] Ricci P, Di Domenico M, Verderame GM. Empirical-based out-of-plane URM infill wall model accounting for the interaction with in-plane demand. Earthq Eng Struct Dyn 2018;47(3):802–27.
[33] Mazza F. In-plane–out-of-plane non-linear model of masonry infills in the seismic analysis of r.c. framed buildings. Earthq Eng Struct Dyn 2019;48(4):432–53.
[34] Mazza F. In-plane and out-of-plane nonlinear seismic response of masonry infills for hospitals retrofitted with hysteretic damped braces. Soil Dyn Earthq Eng 2021;148:106803.
[35] Pekcan G, Mander JB, Chen SS. The seismic response of a 1: 3 scale model R.C. structure with elastomeric spring dampers. Earthq Spectra 1995;11:249–67.
[36] Sorace S, Terenzi G. Non-linear dynamic modelling and design procedure of FV spring-dampers for base isolation. Eng Struct 2001;23:1556–67.
[37] Dyna Shock System. URL ; accessed 23 April 2022.